

Tantalum Cobalt Nitride Photocatalysts for Water Oxidation under Visible Light

Yanqing Cong,[†] Hyun S. Park, Hoang X. Dang, Fu-Ren F. Fan, Allen J. Bard,* and C. Buddie Mullins

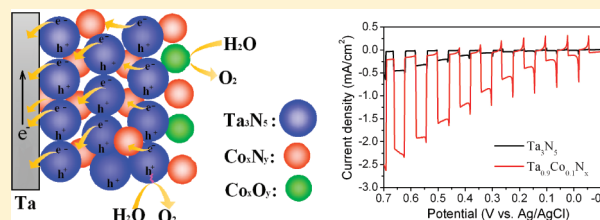
Center for Electrochemistry, Department of Chemistry and Biochemistry, The University of Texas at Austin, 1 University Station A5300, Austin, Texas 78712, United States

Department of Chemical Engineering, Texas Materials Institute, Center for Nano- and Molecular Science, The University of Texas at Austin, 1 University Station C0400, Austin, Texas 78712, United States

Supporting Information

ABSTRACT: Tantalum cobalt nitride photocatalysts were prepared using a simple drop coating method on a Ta foil substrate followed by thermal ammonia treatment, and their photoelectrochemical (PEC) properties for water oxidation under visible light were studied. The resulting $\text{Ta}_{0.9}\text{Co}_{0.1}\text{N}_x$ films showed a photocurrent of ca. 1.5 mA/cm^2 (12 times higher than that of Ta_3N_5) under 100 mW/cm^2 visible light irradiation at 0.7 V vs Ag/AgCl in a 0.1 M Na_2SO_4 aqueous solution (pH 11). The good PEC performance was attributed to the introduction of cobalt and the formation of cobalt nitride, which efficiently facilitates electron transfer and suppresses the recombination of photogenerated electron–hole pairs. Some cobalt nitride could further be oxidized to generate cobalt oxide, which serves as an efficient electrocatalyst for water oxidation. The enhanced visible light activity and film stability under light irradiation make tantalum cobalt nitride a promising semiconductor for PEC water oxidation.

KEYWORDS: tantalum cobalt nitride photocatalysts, photo-oxidation of water, photoelectrochemistry



INTRODUCTION

Photoelectrochemical (PEC) water splitting is a promising method for generating H_2 from solar energy and has attracted much attention as a result of the increasing renewable energy demand.^{1–3} It is especially important to develop a stable semiconductor, which can perform effectively under visible light because 43% of solar energy is in the visible light region.⁴ Much work has been carried out to find band gaps and band positions consistent with high efficiency and water splitting. To utilize visible light, the semiconductor band gap should be smaller than 3 eV (420 nm). In addition, the band energy positions should be suitable for water splitting; the conduction band should be sufficiently negative for H^+ reduction and the valence band sufficiently positive for water oxidation.⁵ However, clearly, other factors are important in gaining good efficiency, for example, establishing conditions for good electron–hole separation, improving carrier mobility, passivating traps, and using electrocatalysts. Although many photocatalysts have been developed in the past decades,^{6–10} efficient and stable photocatalysts responsive to visible light in aqueous solution are still few.

Tantalum nitride (Ta_3N_5) is a good candidate for a PEC catalyst under visible light irradiation and satisfies many of the requirements mentioned: (1) Its band gap is 2.1 eV (absorption edge at 600 nm). (2) At pH 0, its conduction band edge and valence band edge is ca. -0.4 and 1.7 V vs NHE, respectively, well placed for water splitting. (3) It has a theoretical maximum solar spectrum photoconversion efficiency of 15.9%.^{11–13} Domen's group has developed TaON and Ta_3N_5 powders by

heating Ta_2O_5 powder under a NH_3 flow at high temperature, achieving a 34% quantum efficiency (QE) for TaON and 10% for Ta_3N_5 for water oxidation under visible light irradiation.^{14–17} Ta_3N_5 thin films have also been prepared by the nitridation of a Ta_2O_5 film generated on Ta foil. An anodic photocurrent for water oxidation was obtained under visible light irradiation, but some oxidation of Ta_3N_5 itself was also observed. If a solution of $\text{Fe}(\text{CN})_6^{3-}/\text{Fe}(\text{CN})_6^{4-}$ was used as a redox relay instead of water oxidation, Ta_3N_5 was much more stable, with no noticeable surface oxidation. Under monochromatic (wavelength = 450 nm) visible light irradiation, the incident monochromatic photon-to-current conversion efficiency (IPCE) could reach 1.2% in 0.1 M K_2SO_4 solution at pH 11 with a -0.1 V bias vs Ag/AgCl.¹⁸ To further improve the photocatalytic activity, Ta_3N_5 nanoparticles (NPs) were prepared by nitridation of a Ta_2O_5 NPs precursor. Compared to bulk Ta_3N_5 particles, Ta_3N_5 NPs showed enhanced photocatalytic activity, presumably associated with the higher number of surface active sites for hydrogen evolution.¹⁹ Ta_3N_5 NPs synthesized by other methods have been attempted, but the synthetic yield was very low.²⁰ Crystalline mesoporous Ta_3N_5 was prepared from an amorphous mesoporous Ta_2O_5 by nitridation. The crystallized pore thickness of mesoporous Ta_3N_5 was ca. 2 nm, which improved charge transfer of electrons and holes so that the

Received: November 1, 2011

Revised: January 9, 2012

Published: January 9, 2012

photocatalytic activity of mesoporous Ta_3N_5 was 3 times that of conventional bulk Ta_3N_5 .²¹ Domen's group prepared a Ta_3N_5 thin-film using a reactive sputtering technique. The Ta_3N_5 film showed an anodic photoresponse for water oxidation, but self-oxidation of Ta_3N_5 occurred and the photocurrent decreased rapidly with illumination time. IrO_2 modification was used to suppress the self-oxidation of the Ta_3N_5 film and improve the efficiency of water oxidation. Ta_3N_5 films modified with IrO_2 had 30 times higher photocurrent than that of an unmodified sample at 1.0 V bias vs Ag/AgCl .²² Grimes' group fabricated highly oriented Ta_3N_5 nanotube array films by anodization of tantalum foil followed by nitridation. An IPCE as high as 5.3% at 450 nm was achieved for 240 nm long Ta_3N_5 nanotube arrays in 1 M KOH solution with 0.5 V bias.¹²

Although many efforts have been made to optimize the structure and properties of Ta_3N_5 , the promotion of photo-conversion efficiency with good stability of the Ta_3N_5 semiconductor is still challenging. Self-oxidation of Ta_3N_5 needs to be suppressed for water oxidation and novel stable materials are needed overcome these challenges.

In this work, a new tantalum cobalt nitride ($\text{Ta}_y\text{Co}_{1-y}\text{N}_x$) photocatalyst was fabricated on a Ta substrate for water oxidation for the first time. To the best of our knowledge, no previous work regarding the tantalum cobalt nitride or cobalt-doped Ta_3N_5 has been reported. The structural and PEC performance of $\text{Ta}_y\text{Co}_{1-y}\text{N}_x$ electrodes were systematically studied. The photocurrent of $\text{Ta}_{0.9}\text{Co}_{0.1}\text{N}_x$ films increased by 12 times relative to that of Ta_3N_5 films under visible light irradiation. Stability under light illumination was also improved due to the presence of cobalt. Cobalt nitride (Co_xN_y) was found in the $\text{Ta}_y\text{Co}_{1-y}\text{N}_x$ samples, and its role was also investigated.

EXPERIMENTAL SECTION

Preparation of $\text{Ta}_y\text{Co}_{1-y}\text{N}_x$ Films. The $\text{Ta}_y\text{Co}_{1-y}\text{N}_x$ films were prepared by a drop coating method on a Ta foil substrate (Alfa Aesar, 99.95% purity). A 10 mM precursor solution of TaCl_5 (Sigma-Aldrich, 99.99% purity) in methanol (Fisher Scientific, 99.9% purity) was prepared, and 30 μL of the precursor solution was pipetted onto a Ta foil (15 mm \times 15 mm) and then dried in air at room temperature. After repeating this process 10 times, different amounts of a 10 mM solution of $\text{Co}(\text{NO}_3)_2$ (Alfa Aesar, 99.999% purity) in methanol were subsequently dropped onto the same Ta foil, and then, the samples were dried in air at room temperature. The precursor stoichiometric ratios of TaCl_5 to $\text{Co}(\text{NO}_3)_2$ were 9.5/0.5, 9/1, 8/2, and 6/4, and the obtained samples are represented in terms of the precursor ratios as $\text{Ta}_{0.95}\text{Co}_{0.05}\text{N}_x$, $\text{Ta}_{0.9}\text{Co}_{0.1}\text{N}_x$, $\text{Ta}_{0.8}\text{Co}_{0.2}\text{N}_x$, and $\text{Ta}_{0.6}\text{Co}_{0.4}\text{N}_x$, respectively. As shown below, the actual material is a composite with different ratios of Co/Ta than implied by these representations. After drop coating, the samples were annealed in a tube furnace under anhydrous ammonia (Praxair, 99.995% purity) with a flow rate of 100 mL/min at 850 °C for 2 h to produce $\text{Ta}_y\text{Co}_{1-y}\text{N}_x$ films.

To identify the role of Co, two other series of samples were prepared by different methods. One series was Ta_3N_5 films loaded with Co_3O_4 NPs. Ta_3N_5 films were prepared by the same drop coating method. Co_3O_4 NPs were synthesized based on a literature procedure.²³ Briefly, 0.50 g of $\text{Co}(\text{CH}_3\text{COO})_2 \cdot 4\text{H}_2\text{O}$ was dissolved in 25.0 mL of ethanol, and 2.5 mL of 25% ammonia was added under vigorous stirring. After stirring in air for about 10 min, a homogeneous viscous slurry was formed. The suspension was then transferred into a 50.0 mL autoclave, sealed, and maintained at 150 °C for 3 h. After this, the autoclave was cooled to room temperature. The resulting black solid products were washed with ethanol, and the size of the Co_3O_4 NPs was ca. 8 nm. The Ta_3N_5 films were turned up and then immersed in 2 mL of a freshly prepared Co_3O_4 NPs solution (ca. 2 mM) for 3 h. The resulting films ($\text{Ta}_3\text{N}_5/\text{Co}_3\text{O}_4$) were rinsed with Milli-Q deionized (DI) water and dried in air at room temperature. The other series consisted of Co_xN_y

films, which were prepared by the same method on a Co foil substrate (Alfa Aesar, 99.9% purity). A 10 mM precursor solution of $\text{Co}(\text{NO}_3)_2$ in methanol (30 μL) was dropped onto a Co foil (15 mm \times 15 mm) and then dried in air. After repeating this process 10 times, the samples were annealed under an NH_3 flow (100 mL/min) at 850 °C for 2 h to produce films denoted as Co_xN_y .

Characterization. Glancing incidence angle X-ray diffraction (GIXRD) was performed with a Bruker-Norius D8 advanced diffractometer, using a Cu $K\alpha$ radiation source operated at 40 kV and 40 mA, with an incidence angle of 0.5°. Scanning electron microscopy (SEM) images were obtained on a Zeiss Supra 40 VP field emission SEM. X-ray photoelectron spectroscopy (XPS) was performed with a Kratos Axis Ultra DLD instrument (Manchester, UK) with a monochromatic Al X-ray source.

Photoelectrochemical Experiments. The PEC properties of each sample were detected by using a three-electrode borosilicate glass cell equipped with a Pt-gauze counter electrode and an Ag/AgCl reference electrode. A potentiostat (CH Instruments, model 630D, Austin, TX) was used to perform electrochemical measurements. All PEC tests were performed at room temperature. The prepared films were used as working electrodes and were clamped into the glass cell via an O-ring with a 0.2 cm^2 geometric area exposed to the electrolyte solution and to light irradiation. The PEC water oxidation experiments were carried out in 0.1 M Na_2SO_4 solution with pH adjusted to 11 by adding NaOH. Irradiation was achieved through the electrolyte solution by a Xe lamp (XBO 150 W, Osram, Munich, Germany) with an incident UV-visible light intensity of about 110 mW/cm^2 . A UV cutoff filter ($\lambda > 420$ nm) was used for visible light irradiation, and the resulting visible light intensity was ca. 100 mW/cm^2 . A monochromator (Photon Technology International, Birmingham, NJ) was used in combination with a power meter (Newport Model 1830-C, Irvine, CA) and a silicon detector (Newport Model 818-UV, Irvine, CA) to measure incident photon to current conversion efficiencies (IPCE). Electrochemical impedance spectroscopy (EIS) was performed using an Autolab instrument (PGSTAT30/FRA2) to obtain the Mott-Schottky plot at frequencies of 200, 500, and 1000 Hz and a peak-to-peak amplitude of 5 mV at each potential.

RESULTS AND DISCUSSION

Characterization of $\text{Ta}_y\text{Co}_{1-y}\text{N}_x$ Films. GIXRD analyses were used to identify the crystal phase of $\text{Ta}_y\text{Co}_{1-y}\text{N}_x$ films. To assign the diffraction peaks, a sample of $\text{Ta}_{0.6}\text{Co}_{0.4}\text{N}_x$ was prepared; the XRD pattern is shown in Figure 1. The main phases identified are orthorhombic-phase Ta_3N_5 and cubic-phase $\text{Co}_{5.47}\text{N}$. Some hexagonal-phase $\text{Ta}\text{N}_{0.43}$ is formed as an intermediate phase because NH_3 gas permeates through the film to the Ta substrate. No characteristic peaks corresponding to a tantalum cobalt nitride were identified. The GIXRD patterns of the films prepared with other Ta/Co ratios are given in Figure 2. To avoid the effect of the Ta substrate, the Co_xN_y sample was prepared on a Co foil by annealing a $\text{Co}(\text{NO}_3)_2$ precursor in an NH_3 flow. Cobalt nitride was formed, and the diffraction peaks of samples are assigned to be cubic-phase and hexagonal-phase (XRD patterns are shown in Figure S1 in the Supporting Information). In Figure 2, compared to a Ta_3N_5 film, the XRD peaks of $\text{Ta}_y\text{Co}_{1-y}\text{N}_x$ films have no obvious shift with the increase in Co content. Several peaks in tantalum nitride overlap with the peaks of cobalt nitride. If we focus on the 43.8° 2θ peak (Figure 2b), some cobalt nitride appears to exist as a separate phase. However, the changes are not obvious, even though samples with high Co content were used. It is hard to determine whether some cobalt nitride is incorporated into the tantalum nitride.

Figure 3 shows the SEM images of a $\text{Ta}_{0.8}\text{Co}_{0.2}\text{N}_x$ film annealed under an NH_3 flow at 850 °C. The measurements were carried out on mechanically scraped-off samples, whereon

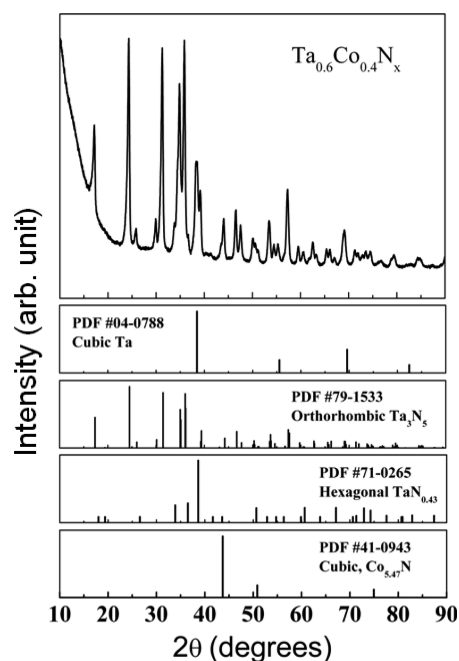


Figure 1. GIXRD pattern of tantalum cobalt nitride film prepared on Ta substrate under NH_3 treatment. Representative diffraction pattern (upper) and corresponding standard JCPDS patterns (lower).

a part of the films had peeled off. The film is uniform, and the thickness is approximately $1 \mu\text{m}$. No features of cobalt nitride are seen from the morphologies. The structure of the $\text{Ta}_{0.8}\text{Co}_{0.2}\text{N}_x$ film is somewhat porous, indicating that the PEC behavior might be improved because the film has a greater surface area in contact with the solution. Although the film is generally uniform, some cracks still existed on the surface of the films (see Figure S2 in the Supporting Information).

Photocatalytic Activity. The PEC performance of tantalum cobalt nitride films was studied using linear sweep voltammetry (LSV). Figure 4 shows the LSVs of Ta_3N_5 and $\text{Ta}_{0.9}\text{Co}_{0.1}\text{N}_x$ films in $0.1 \text{ M Na}_2\text{SO}_4$ aqueous solution (pH 11) under chopped (a) UV–visible and (b) visible ($\lambda > 420 \text{ nm}$) light irradiation. $\text{Ta}_{0.9}\text{Co}_{0.1}\text{N}_x$ films exhibited a significant increase in photocurrent relative to Ta_3N_5 . The photocurrent of $\text{Ta}_{0.9}\text{Co}_{0.1}\text{N}_x$ was ca. 5 times higher under UV–visible light irradiation and 12 times higher under visible light irradiation than that of Ta_3N_5 at 0.7 V vs Ag/AgCl . The enhancements were even higher in the region of less positive potentials. Because Ta_3N_5 is an insulating n-type semiconductor, an excessive anodic overpotential was needed to obtain a high photocurrent.¹⁸ The presence of cobalt in $\text{Ta}_{0.9}\text{Co}_{0.1}\text{N}_x$ films not only promotes the oxidation of water, but also could lower the anodic overpotential of Ta_3N_5 to obtain larger photocurrent.

Effect of Cobalt Content. The composition of $\text{Ta}_y\text{Co}_{1-y}\text{N}_x$ films was examined to investigate the effects of cobalt content on the oxidation of water. Figure 5 shows the LSVs of films prepared with various Ta/Co precursor stoichiometries in $0.1 \text{ M Na}_2\text{SO}_4$ aqueous solution (pH 11). Even with a large Ta/Co ratio ($\text{Ta}_{0.95}\text{Co}_{0.05}\text{N}_x$), the photocurrent can reach $0.3 \text{ mA}/\text{cm}^2$ under visible light irradiation at 0.4 V potential bias vs Ag/AgCl (Figure 5b), which is ca. 7 times higher than that of Ta_3N_5 . When the cobalt content was 10% ($\text{Ta}_{0.9}\text{Co}_{0.1}\text{N}_x$), the photocurrent reached $1.3 \text{ mA}/\text{cm}^2$ (UV–visible light irradiation at $110 \text{ mW}/\text{cm}^2$) and $0.75 \text{ mA}/\text{cm}^2$ ($>420 \text{ nm}$ visible light irradiation at $100 \text{ mW}/\text{cm}^2$) at 0.4 V bias, which is near the thermodynamic potential for water oxidation at pH 11. However, with increasing bias to 0.7 V , the photocurrent could reach $2.3 \text{ mA}/\text{cm}^2$ (UV–visible light irradiation) and $1.4 \text{ mA}/\text{cm}^2$ (visible light irradiation). As the cobalt content was increased, for example, for a $\text{Ta}_{0.6}\text{Co}_{0.4}\text{N}_x$ sample, the photocurrent showed only a slight enhancement under UV–visible and visible irradiation relative

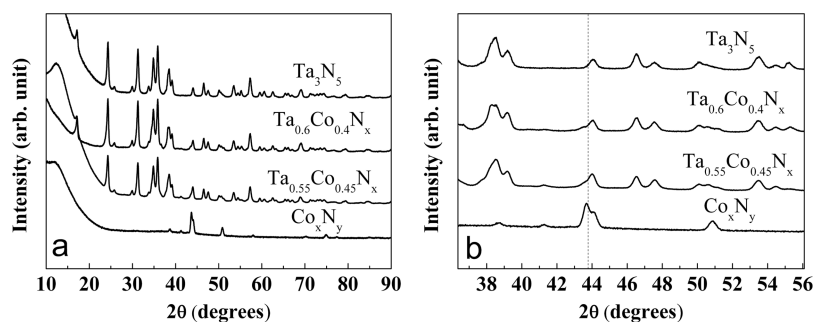


Figure 2. GIXRD patterns of $\text{Ta}_y\text{Co}_{1-y}\text{N}_x$ films prepared with various Ta/Co ratios.

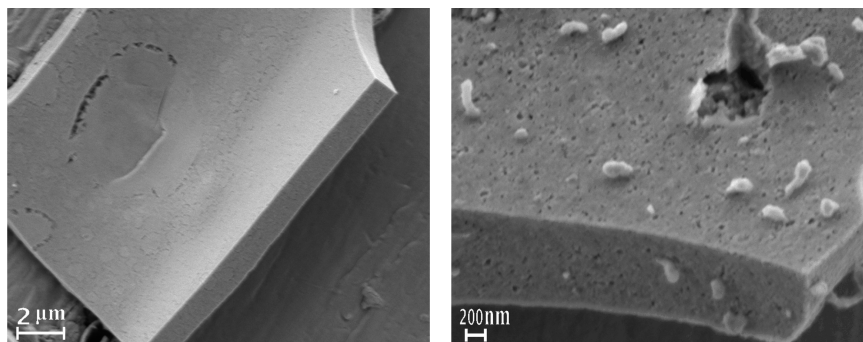


Figure 3. SEM images of $\text{Ta}_{0.8}\text{Co}_{0.2}\text{N}_x$ flakes on a Ta substrate. The samples were nitrided at $850 \text{ }^\circ\text{C}$ for 2 h in an NH_3 gas flow of $100 \text{ mL}/\text{min}$.

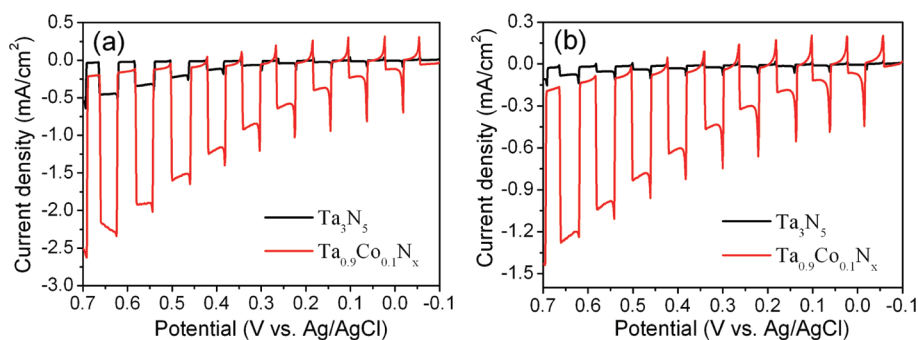


Figure 4. Linear sweep voltammograms of Ta_3N_5 and $\text{Ta}_{0.9}\text{Co}_{0.1}\text{N}_x$ films in 0.1 M Na_2SO_4 aqueous solution (pH 11) under chopped UV–visible (a) and visible (b) light irradiation. Scan from -0.1 to 0.7 at 20 mV/s. Light intensity: 110 mW/cm² (150W Xe lamp). The thermodynamic potential for water oxidation is 0.39 V vs Ag/AgCl at pH 11.

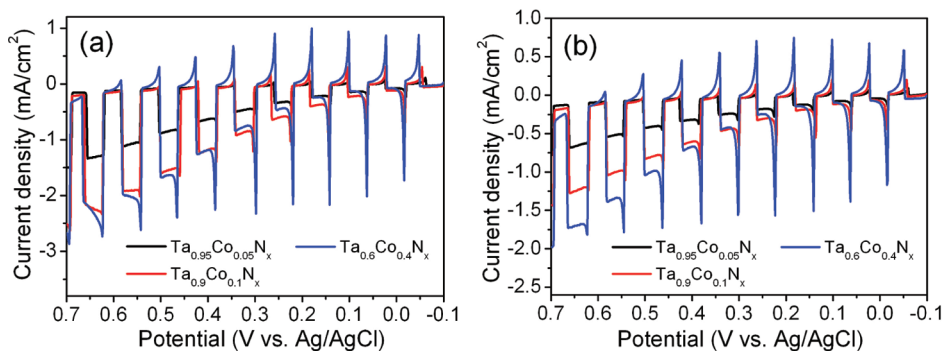


Figure 5. Linear sweep voltammograms of $\text{Ta}_y\text{Co}_{1-y}\text{N}_x$ films prepared with various Ta/Co ratios in 0.1 M Na_2SO_4 aqueous solution (pH 11) under chopped UV–visible (a) and visible (b) light irradiation. Scan rate: 20 mV/s. Light intensity: 110 mW/cm² (150W Xe lamp).

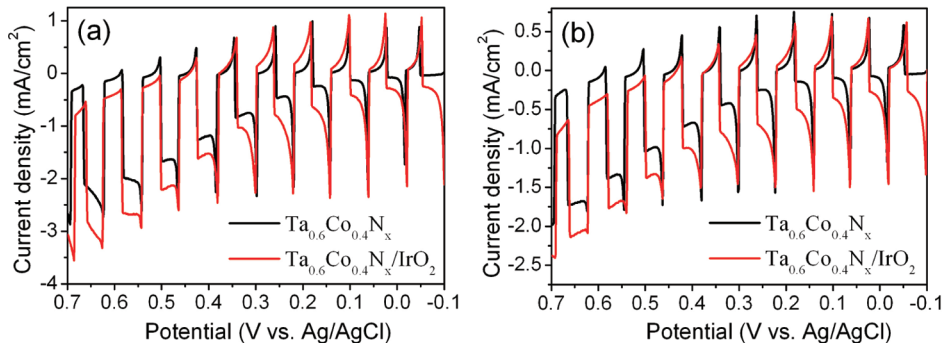


Figure 6. Linear sweep voltammograms of $\text{Ta}_{0.6}\text{Co}_{0.4}\text{N}_x$ and $\text{Ta}_{0.6}\text{Co}_{0.4}\text{N}_x/\text{IrO}_2$ films in 0.1 M Na_2SO_4 aqueous solution (pH 11) under chopped UV–visible (a) and visible (b) light irradiation. Scan rate: 20 mV/s. Light intensity: 110 mW/cm² (150W Xe lamp).

to that of $\text{Ta}_{0.9}\text{Co}_{0.1}\text{N}_x$ with apparent higher recombination peaks. A further increase in cobalt content brought about a deterioration of photocurrent. In addition, for samples with high cobalt content, the magnitudes of the current transients associated with either light-on or light-off switching were large, suggesting that larger recombination processes were involved. If an aqueous solution containing a sacrificial reagent (e.g., hydroquinone) was used to scavenge the photogenerated charge carriers in the PEC experiments, the current transients during light-chopping periods were significantly suppressed and $\text{Ta}_{0.6}\text{Co}_{0.4}\text{N}_x$ showed considerably higher photocurrents relative to that of $\text{Ta}_{0.9}\text{Co}_{0.1}\text{N}_x$ (Figure S3 in the Supporting Information).

A rapid oxygen evolution reaction (OER) is difficult to achieve because the OER involves a complicated four electron, four proton process and occurs with high overpotential, even with good electrocatalysts. It is especially challenging for

photocatalysts with small band gaps, where the valence band potential is not very positive. To facilitate the investigation of the performance of $\text{Ta}_y\text{Co}_{1-y}\text{N}_x$ films for the OER, IrO_2 was loaded on the surface of $\text{Ta}_y\text{Co}_{1-y}\text{N}_x$ films. IrO_2 is known to be a good electrocatalyst for water oxidation on metal and carbon electrodes.^{24,25} A colloidal solution of IrO_2 was prepared by hydrolysis of K_2IrCl_6 (Alfa Aesar) in aqueous basic solution.⁹ The K_2IrCl_6 solution was adjusted to pH 12 using NaOH, then heated at 70 °C for 30 min in air. After cooling to room temperature, the solution was adjusted to pH 9 with HNO_3 to obtain a colloidal IrO_2 solution. The $\text{Ta}_{0.6}\text{Co}_{0.4}\text{N}_x$ electrode was immersed into the prepared IrO_2 solution for 3 h, washed with DI water, and then dried in air (represented as $\text{Ta}_{0.6}\text{Co}_{0.4}\text{N}_x/\text{IrO}_2$). Figure 6 shows the LSVs of $\text{Ta}_{0.6}\text{Co}_{0.4}\text{N}_x$ and $\text{Ta}_{0.6}\text{Co}_{0.4}\text{N}_x/\text{IrO}_2$ films in 0.1 M Na_2SO_4 aqueous solution (pH 11). The IrO_2 modification on $\text{Ta}_{0.6}\text{Co}_{0.4}\text{N}_x$ films significantly improves the

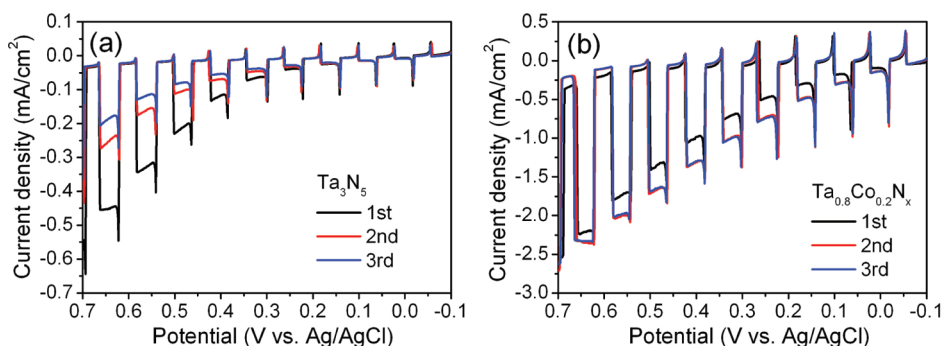


Figure 7. Linear sweep voltammograms of Ta_3N_5 (a) and $\text{Ta}_{0.8}\text{Co}_{0.2}\text{N}_x$ (b) films in 0.1 M Na_2SO_4 aqueous solution (pH 11) under chopped UV–visible light irradiation. Scan rate: 20 mV/s. Light intensity: 110 mW/cm^2 (150W Xe lamp).

photocurrent for water oxidation, especially in the region of low potential. Because cobalt oxides are known to be good electrocatalysts for the OER,^{26–28} the observed current transients of high cobalt content samples are probably associated with facilitating water oxidation.

Stability. As mentioned earlier,^{21,22} Ta_3N_5 is unstable during photocatalytic water oxidation because of the self-oxidation of Ta_3N_5 by photogenerated holes. To study the stability of prepared $\text{Ta}_y\text{Co}_{1-y}\text{N}_x$ films, LSVs of the same samples were repeated 3 times, and the results are shown in Figure 7. The photocurrent of the Ta_3N_5 electrode decayed rapidly by 45% in a second sweep, demonstrating the instability of Ta_3N_5 (Figure 7a). For a $\text{Ta}_{0.9}\text{Co}_{0.1}\text{N}_x$ film, the photocurrent slowly decreases by 12% in the second sweep (see Figure S4 in the Supporting Information). When the cobalt content was increased to 20% ($\text{Ta}_{0.8}\text{Co}_{0.2}\text{N}_x$), the photocurrent actually increased in the second sweep, then remained stable in the third sweep (Figure 7b). One possible reason for the photocurrent increase of the $\text{Ta}_y\text{Co}_{1-y}\text{N}_x$ electrode with high cobalt content in the second sweep is that some cobalt nitride was oxidized by photogenerated holes to form cobalt oxide (an electrocatalyst for the OER), which could remove more rapidly photogenerated holes from the surface. Similar results were obtained for other films having a high cobalt content. This indicates that the stability of $\text{Ta}_y\text{Co}_{1-y}\text{N}_x$ films can be improved and self-oxidation of Ta_3N_5 suppressed when cobalt nitride is incorporated into Ta_3N_5 films. For comparison, Ta_3N_5 films loaded with Co_3O_4 NPs were prepared, and the LSVs under the same conditions are shown in Figure S5 in the Supporting Information. No increased photocurrent was observed in the second sweep and photocurrents decreased with the sweep times.

To confirm that the photocurrent observed at low potential involved the OER, PEC experiments were carried out at a fixed low potential, e.g., 0.0 V vs Ag/AgCl. Oxygen bubbles were generated and clearly observed on the surface of the tested $\text{Ta}_{0.8}\text{Co}_{0.2}\text{N}_x$ electrode after long-time irradiation (Figure S6 in the Supporting Information). After a 14 h irradiation, LSVs of the same electrode were recorded, and the results are shown in Figure 8. After long-time continuous irradiation, the photocurrent of the $\text{Ta}_{0.8}\text{Co}_{0.2}\text{N}_x$ electrode had decreased to ca. 0.8 mA/cm^2 at 0.7 V bias. However, the photocurrent and stability of this used $\text{Ta}_{0.8}\text{Co}_{0.2}\text{N}_x$ electrode was still better than that of a fresh Ta_3N_5 .

XPS measurements were performed to analyze the chemical composition and oxidation state of each element at the electrode surface. $\text{Ta}_{0.6}\text{Co}_{0.4}\text{N}_x$ samples with high cobalt content were used to obtain stronger Co peaks. As shown in Figure 9, the Ta (4f), Co (2p), N (1s), and O (1s) peaks confirmed the presence

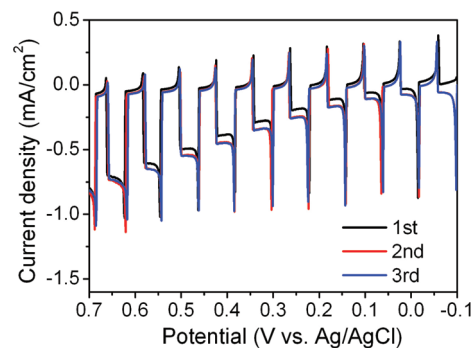


Figure 8. Linear sweep voltammograms at a $\text{Ta}_{0.8}\text{Co}_{0.2}\text{N}_x$ electrode in 0.1 M Na_2SO_4 aqueous solution (pH 11) after 14 h UV–visible light irradiation. Light intensity: 110 mW/cm^2 (150W Xe lamp). The potential was kept at 0.0 V vs Ag/AgCl. Scan rate: 20 mV/s.

of each element. The contaminating C (1s) peak at 285.15 eV was used as a standard to calibrate the binding energies. After irradiation for 14 h at 0.7 V potential in 0.1 M Na_2SO_4 aqueous solution (pH 11), the Ta4f7/2 peak shifts from 25.05 to 26.35 eV, which corresponds to the transformation of Ta_3N_5 to Ta_2O_5 .^{18,26} A shoulder (between 25 and 26 eV) in the Ta4f7/2 peak is observed for the sample after the stability experiment, which can be attributed to suboxides. For thick films, the suboxides are present as heterogeneities in Ta_2O_5 bulk films, but their amount is quite small based on the shoulder intensity from the XPS measurements.²⁹ The intensity of N (1s) peaks decreased, and that of O (1s) peaks increased after the experiments. No significant change in Co (2p) peaks was observed. All the changes regarding Ta, N, and O peaks indicate that some Ta_3N_5 was oxidized to generate Ta_2O_5 or TaON under long-time irradiation. As a result of the large band gap of Ta_2O_5 (3.9 eV), the photocurrent of the $\text{Ta}_y\text{Co}_{1-y}\text{N}_x$ electrode decreased (Figure 8). For comparison, a $\text{Ta}_{0.6}\text{Co}_{0.4}\text{N}_x$ electrode after irradiation for 30 min under the same conditions was analyzed, and the XPS spectra are shown in Figure S7 in the Supporting Information. No significant shift in the Ta (4f) peak was observed. The N (1s) peaks have a slight decrease after irradiation for 30 min. The Co (2p) peaks and O (1s) peaks have no significant changes. Table 1 summarizes the atomic ratios of N/Ta, O/Ta and Co/Ta on the surface of the $\text{Ta}_{0.6}\text{Co}_{0.4}\text{N}_x$ electrode, calculated from the areas of the XPS spectra before and after irradiation at 0.7 V in 0.1 M Na_2SO_4 aqueous solution (pH 11). The measured N/Ta ratio is small relative to the stoichiometry for Ta_3N_5 , and additionally, oxygen exists in the fresh sample. The atomic ratio for Co/Ta is also less than that in the precursor stoichiometry. The results in

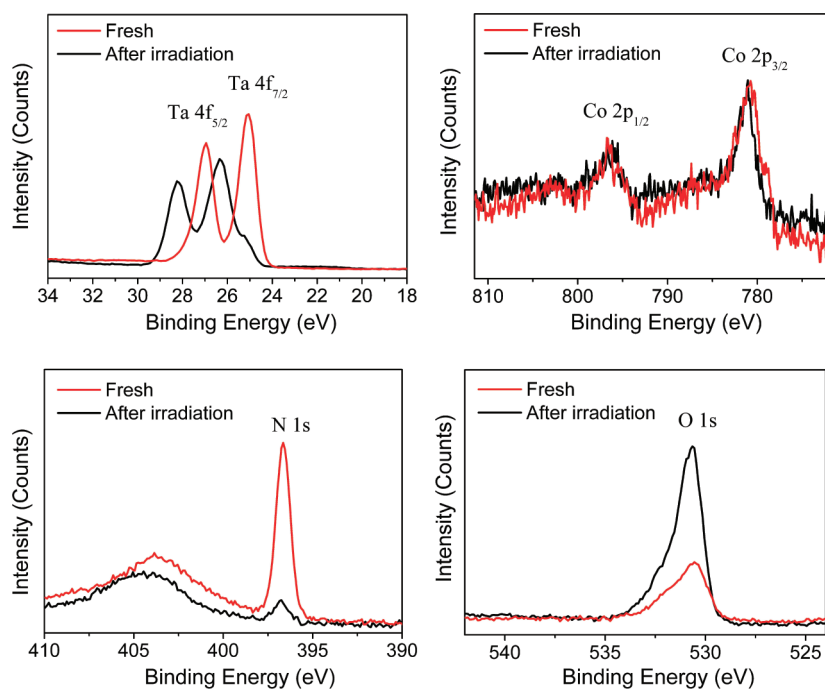


Figure 9. XPS spectra of a $\text{Ta}_{0.6}\text{Co}_{0.4}\text{N}_x$ electrode before (red) and after (black) UV–visible light irradiation (14 h) in 0.1 M Na_2SO_4 aqueous solution (pH 11). Light intensity: $110 \text{ mW}/\text{cm}^2$ (150W Xe lamp). The potential was kept at 0.7 V vs Ag/AgCl.

Table 1. Atomic Ratios of N/Ta, O/Ta, and Co/Ta in $\text{Ta}_{0.6}\text{Co}_{0.4}\text{N}_x$ Electrode

	N/Ta	O/Ta	Co/Ta
precursor stoichiometry	1.67		0.66
fresh sample (XPS)	1.4	0.8	0.34
after irradiation for 30 min ^a (XPS)	1.22	1.0	0.39
after irradiation for 14 h ^a (XPS)	0.36	2.2	0.45

^aAt 0.7 V vs Ag/AgCl in 0.1 M Na_2SO_4 aqueous solution (pH 11) under irradiation of $110 \text{ mW}/\text{cm}^2$ (150W Xe lamp).

Figures 7 and 9, as well as Figure S6 in the Supporting Information, suggest that the presence of cobalt nitride facilitates PEC water oxidation and stability of Ta_3N_5 , but some degradation of $\text{Ta}_y\text{Co}_{1-y}\text{N}_x$ is still observed. Further effort is required to optimize the structure and performance of $\text{Ta}_y\text{Co}_{1-y}\text{N}_x$ films.

IPCE. Figure 10 shows the IPCE plots as functions of wavelength for $\text{Ta}_y\text{Co}_{1-y}\text{N}_x$ films with different cobalt contents calculated by the equation:

$$\text{IPCE} (\%) = 1240(i_{\text{ph}}/\lambda P_{\text{in}}) \times 100$$

where i_{ph} is the photocurrent (mA), λ is the wavelength (nm) of incident radiation, and P_{in} is the incident light power intensity on the semiconductor electrode at the selected wavelength (mW).⁵ The calculated IPCE values for a $\text{Ta}_{0.6}\text{Co}_{0.4}\text{N}_x$ electrode are up to 25% at 450 nm in 0.1 M Na_2SO_4 aqueous solution (pH 11) at 0.6 V vs Ag/AgCl. The IPCE values decrease with increasing wavelength and are essentially negligible beyond $\sim 600 \text{ nm}$ for both Ta_3N_5 and $\text{Ta}_y\text{Co}_{1-y}\text{N}_x$ films, indicating that there is no significant difference in the band gap energy of these $\text{Ta}_y\text{Co}_{1-y}\text{N}_x$ films, estimated as about 2.1 eV.

Mott–Schottky Plots. $\text{Ta}_y\text{Co}_{1-y}\text{N}_x$ films were analyzed by electrochemical impedance spectroscopy. Experiments were carried out in 0.1 M Na_2SO_4 solution (pH 11) at frequencies of

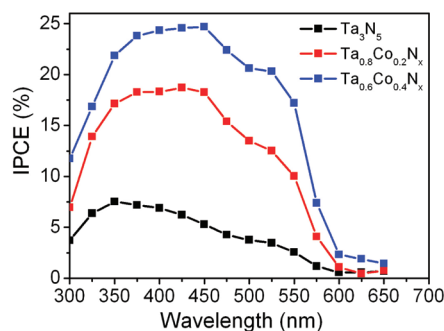


Figure 10. IPCE plot of $\text{Ta}_y\text{Co}_{1-y}\text{N}_x$ films having various cobalt content calculated from the photocurrents in 0.1 M Na_2SO_4 aqueous solution (pH 11) at an applied potential of 0.6 V vs Ag/AgCl.

500, 1000, and 3000 Hz in the dark. The Mott–Schottky (MS) plots of Ta_3N_5 and $\text{Ta}_{0.8}\text{Co}_{0.2}\text{N}_x$ films are shown in Figure 11. If the space-layer capacitance, C_{SC} , of the semiconductor is much smaller than the double-layer capacitance at the semiconductor/electrolyte interface and no faradaic processes, including pseudocapacitance and surface state charging, are involved, C_{SC} can be approximated by the measured overall capacitance, C . In such an ideal case, linear MS plots (i.e., $1/C^2$ vs potential plots) can be obtained, and they supply information on the doping density and the flat band potential, E_{fb} , of the semiconductor. As shown in Figure 11, the MS plot of each film has a slope that is consistent with the behavior of an n-type semiconductor. The reason for the frequency dispersion shown is not clear and needs to be investigated further. The band edges of Ta_3N_5 are reported to shift linearly with the pH by 60 mV per pH unit change in the solution.¹³ The E_{fb} of Ta_3N_5 is approximated to be -0.93 V vs Ag/AgCl at pH = 11 (ca. -0.05 V vs NHE (pH = 0)). The estimated E_{fb} of $\text{Ta}_{0.8}\text{Co}_{0.2}\text{N}_x$ is -0.85 V vs Ag/AgCl in 0.1 M Na_2SO_4 solution (pH 11). Figure S8 in the Supporting Information shows the LSVs of Ta_3N_5 and $\text{Ta}_{0.8}\text{Co}_{0.2}\text{N}_x$ films in 0.1 M Na_2SO_4

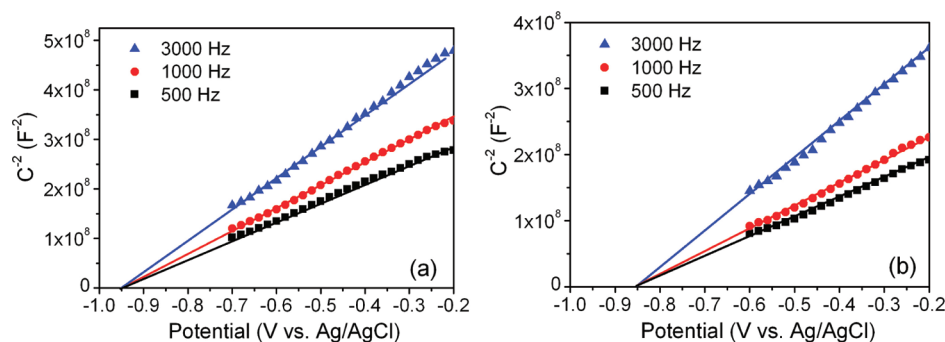


Figure 11. Mott–Schottky plots of Ta_3N_5 (a) and $\text{Ta}_{0.8}\text{Co}_{0.2}\text{N}_x$ (b) in 0.1 M Na_2SO_4 aqueous solution (pH 11) under dark condition with an AC amplitude of 5 mV at each potential.

aqueous solution (pH 11) under chopped UV–visible light irradiation and in the dark. The apparent onset potentials of anodic photocurrents of Ta_3N_5 and $\text{Ta}_{0.8}\text{Co}_{0.2}\text{N}_x$ films correspond to the respective E_{fb} . A similar E_{fb} for Ta_3N_5 was also observed in earlier studies.¹⁸ The small difference in the value for E_{fb} between Ta_3N_5 and $\text{Ta}_{0.8}\text{Co}_{0.2}\text{N}_x$ may be a contributing factor in the photocurrent enhancement of $\text{Ta}_y\text{Co}_{1-y}\text{N}_x$ vs Ta_3N_5 films.

Although these measurements place E_{fb} at about -0.8 V. vs Ag/AgCl, the photocurrent only increases slowly and nearly linearly with increasing positive potential (i.e., it behaves as essentially a constant high-resistance device), with appreciable IPCE values only obtained in the 0.2 to 0.6 V vs Ag/AgCl region. This suggests that improvements in carrier velocity and concentration and decreases in recombination rates might provide significant improvements in the performance of this material.

Possible Mechanism. The higher PEC water oxidation activity of $\text{Ta}_y\text{Co}_{1-y}\text{N}_x$ electrodes is apparently associated with the incorporation of cobalt and the resulting formation of Co_xN_y , a conductive, magnetic, interstitial type transition metal compound³⁰ that is synthesized by reactive sputtering and the ammonia nitridation method.^{31–33} The resistivity of Co_xN_y prepared in this work was measured using a collinear four point probe. The sheet resistivity of Co_xN_y samples is ~ 0.049 Ω/square . The resistivity of Ta_3N_5 and $\text{Ta}_y\text{Co}_{1-y}\text{N}_x$ films could not be obtained reliably because it is outside the probe’s measurement limits. The function of Co_xN_y could be attributed to different factors: First, as a conductor, Co_xN_y serves as the acceptor of electrons produced in Ta_3N_5 and efficiently accelerates the electron transfer. Due to the good conductivity of Co_xN_y , the recombination of photogenerated electron–hole pairs could be significantly suppressed, leaving more holes to oxidize the water; however, it might also serve as a recombination center through intermolecular electron transfer. Second, the incorporation of Co_xN_y slightly changed the E_{fb} of the materials in a positive direction, while no significant band gap change was observed, which might also improve the kinetic for water oxidation. Third, some of the Co_xN_y could be oxidized by photogenerated holes to generate some cobalt oxide, which can serve as a good electrocatalyst for water oxidation. A schematic of a tentative mechanism is shown in Figure 12. Under irradiation, electrons are excited from the valence band into the conduction band of Ta_3N_5 . Because Co_xN_y is introduced into the Ta_3N_5 semiconductor, photogenerated electrons could be rapidly transported and separated from the holes. There are more holes to react with water, thus a higher efficiency for PEC water oxidation can be achieved. In addition, some oxidized Co_xN_y

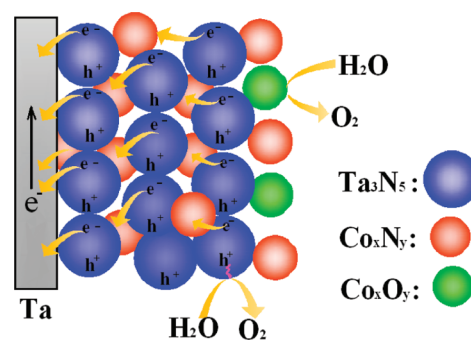


Figure 12. Schematic of the charge separation and electron transport in $\text{Ta}_y\text{Co}_{1-y}\text{N}_x$ films under irradiation.

may provide some active sites of an electrocatalyst for water oxidation. Note that a suitable cobalt content is crucial for obtaining high PEC efficiency. The Co sites in $\text{Ta}_y\text{Co}_{1-y}\text{N}_x$ electrodes with too high a cobalt content could become the recombination centers of hole–electron pairs and decrease the PEC performance. Thus, this study illustrates the application of dopants in improving the performance of a semiconductor photocatalyst, even without major changes in the band gap or band positions and the need to optimize the dopant concentration.

CONCLUSIONS

Tantalum cobalt nitride photocatalysts have been successfully fabricated by a simple drop coating method followed by ammonia treatment. The introduction of cobalt in $\text{Ta}_{0.9}\text{Co}_{0.1}\text{N}_x$ films not only improved the photocurrent by about 12 times under visible light irradiation relative to that of Ta_3N_5 at 0.7 V vs Ag/AgCl in 0.1 M Na_2SO_4 aqueous solution (pH 11) but also the addition of cobalt also lowered the anodic overpotential for water oxidation. After thermal nitridation, the films, denoted as $\text{Ta}_y\text{Co}_{1-y}\text{N}_x$, are composed of tantalum nitride and cobalt nitride. Cobalt nitride is suggested to facilitate electron transfer and suppress the recombination of photogenerated electron–hole pairs. Therefore, the stability of the $\text{Ta}_y\text{Co}_{1-y}\text{N}_x$ films was significantly improved compared to Ta_3N_5 , and its self-oxidation was suppressed. Furthermore, some cobalt nitride could be oxidized by photogenerated holes to generate cobalt oxide, which can serve as an electrocatalyst for the oxidation of water. The results demonstrate that tantalum cobalt nitride is a promising semiconducting composite material for utilizing visible light for PEC application for water oxidation.

■ ASSOCIATED CONTENT

■ Supporting Information

Additional supporting figures. This material is available free of charge via the Internet at <http://pubs.acs.org>.

■ AUTHOR INFORMATION

Corresponding Author

*E-mail: ajbard@mail.utexas.edu.

Present Address

†Permanent Address: College of Environmental Science and Engineering, Zhejiang Gongshang University, Hangzhou, 310012, China

■ ACKNOWLEDGMENTS

This work was financially supported by the National Science Foundation (CHE-0934450) and the Robert A. Welch Foundation (Grant No. F-1436 for CBM and Grant No. F-0021 for AJB). Y.C. Cong thanks the Zhejiang Provincial Natural Science Foundation of China (No. R5100266), the National Science Foundation of China (No. 20976162) and the National Scholarship Fund of China Scholarship Council (No. 2009833095) for support. H.X. Dang acknowledges the Viet Nam Education Foundation (VEF) for support. We also thank Dr. Sung Ki Cho for XPS measurements.

■ REFERENCES

- (1) Walter, M. G.; Warren, E. L.; McKone, J. R.; Boettcher, S. W.; Mi, Q. X.; Santori, E. A.; Lewis, N. S. *Chem. Rev.* **2010**, *110*, 6446.
- (2) Bard, A. J.; Fox, M. A. *Acc. Chem. Res.* **1995**, *28*, 141.
- (3) Gratzel, M. *Nature* **2001**, *414*, 338.
- (4) Li, Q.; Guo, B. D.; Yu, J. G.; Ran, J. R.; Zhang, B. H.; Yan, H. J.; Gong, J. R. *J. Am. Chem. Soc.* **2011**, *133*, 10878.
- (5) Ye, H.; Lee, J.; Jang, J. S.; Bard, A. J. *J. Phys. Chem. C* **2010**, *114*, 13322.
- (6) Park, J. H.; Kim, S.; Bard, A. J. *Nano Lett.* **2006**, *6*, 24.
- (7) Zou, Z. G.; Ye, J. H.; Sayama, K.; Arakawa, H. *Nature* **2001**, *414*, 625.
- (8) Chen, X. B.; Liu, L.; Yu, P. Y.; Mao, S. S. *Science* **2011**, *331*, 746.
- (9) Abe, R.; Higashi, M.; Domen, K. *J. Am. Chem. Soc.* **2010**, *132*, 11828.
- (10) Kudo, A.; Miseki, Y. *Chem. Soc. Rev.* **2009**, *38*, 253.
- (11) Tabata, M.; Maeda, K.; Higashi, M.; Lu, D. L.; Takata, T.; Abe, R.; Domen, K. *Langmuir* **2010**, *26*, 9161.
- (12) Feng, X. J.; LaTempa, T. J.; Basham, J. I.; Mor, G. K.; Varghese, O. K.; Grimes, C. A. *Nano Lett.* **2010**, *10*, 948.
- (13) Chun, W. J.; Ishikawa, A.; Fujisawa, H.; Takata, T.; Kondo, J. N.; Hara, M.; Kawai, M.; Matsumoto, Y.; Domen, K. *J. Phys. Chem. B* **2003**, *107*, 1798.
- (14) Lu, D. L.; Hitoki, G.; Katou, E.; Kondo, J. N.; Hara, M.; Domen, K. *Chem. Mater.* **2004**, *16*, 1603.
- (15) Hitoki, G.; Ishikawa, A.; Takata, T.; Kondo, J. N.; Hara, M.; Domen, K. *Chem. Lett.* **2002**, *7*, 736.
- (16) Maeda, K.; Higashi, M.; Lu, D. L.; Abe, R.; Domen, K. *J. Am. Chem. Soc.* **2010**, *132*, 5858.
- (17) Lee, Y.; Nukumizu, K.; Watanabe, T.; Takata, T.; Hara, M.; Yoshimura, M.; Domen, K. *Chem. Lett.* **2006**, *35*, 352.
- (18) Ishikawa, A.; Takata, T.; Kondo, J. N.; Hara, M.; Domen, K. *J. Phys. Chem. B* **2004**, *108*, 11049.
- (19) Maeda, K.; Nishimura, N.; Domen, K. *Appl. Catal., A* **2009**, *370*, 88.
- (20) Ho, C. T.; Low, K. B.; Klie, R. F.; Maeda, K.; Domen, K.; Meyer, R. J.; Snee, P. T. *J. Phys. Chem. C* **2011**, *115*, 647.
- (21) Hisatomi, T.; Otani, M.; Nakajima, K.; Teramura, K.; Kako, Y.; Lu, D. L.; Takata, T.; Kondo, J. N.; Domen, K. *Chem. Mater.* **2010**, *22*, 3854.

- (22) Yokoyama, D.; Hashiguchi, H.; Maeda, K.; Minegishi, T.; Takata, T.; Abe, R.; Kubota, J.; Domen, K. *Thin Solid Films* **2011**, *519*, 2087.
- (23) Dong, Y.; He, K.; Yin, L.; Zhang, A. *Nanotechnology* **2007**, *18*, 435602.
- (24) Hackwood, S.; Schiavone, L. M.; Dautremontsmith, W. C.; Beni, G. *J. Electrochem. Soc.* **1981**, *128*, 2569.
- (25) Hara, M.; Waraksa, C. C.; Lean, J. T.; Lewis, B. A.; Mallouk, T. E. *J. Phys. Chem. A* **2000**, *104*, 5275.
- (26) Jiao, F.; Frei, H. *Angew. Chem., Int. Ed.* **2009**, *48*, 1841.
- (27) Yeo, B. S.; Bell, A. T. *J. Am. Chem. Soc.* **2011**, *133*, 5587.
- (28) Esswein, A. J.; McMurdo, M. J.; Ross, P. N.; Bell, A. T.; Tilley, T. D. *J. Phys. Chem. C* **2009**, *113*, 15068.
- (29) Kerrec, O.; Devilliers, D.; Groult, H.; Marcus, P. *Mater. Sci. Eng.* **1998**, *B55*, 134.
- (30) Matsuoka, M.; Ono, K.; Inukai, T. *Appl. Phys. Lett.* **1986**, *49*, 977.
- (31) Su, C. W.; Huang, M. S.; Chang, Y. C.; Tsai, T. H.; Lee, Lee, J. C. *J. Appl. Phys.* **2009**, *105*, 033509.
- (32) Suzuki, K.; Kaneko, T.; Yoshida, H.; Morita, H.; Fujimori, H. *J. Alloys Compd.* **1995**, *224*, 232.
- (33) Shi, Y. R.; Wan, Y.; Zhang, R. Y.; Zhao, D. Y. *Adv. Funct. Mater.* **2008**, *18*, 2436.